Polymer Chemistry

Polymersome formation induced by encapsulation of water-insoluble molecules within ABC triblock terpolymers

Journal:	*Polymer Chemistry*
Manuscript ID	PY-ART-03-2020-000426.R1
Article Type:	Paper
Date Submitted by the Author:	15-Apr-2020
Complete List of Authors:	Takahashi, Rintaro; University of Kitakyushu, Department of Chemistry and Biochemistry Miwa, Shotaro; The University of Kitakyushu, Rössel, Carsten; Friedrich Schiller University Jena, b. Institute of Organic Chemistry and Macromolecular Chemistry Fujii, Shota; University of Kitakyushu, Lee, Ji Ha; University of Kitakyushu, Department of Chemistry and Biochemistry Schacher, Felix; Friedrich Schiller University Jena, Institute of Organic and Macromolecular Chemistry Sakurai, Kazuo ; University of Kitakyushu, Dep. of Chemistry & Biochemistry

ARTICLE

Polymersome formation induced by encapsulation of water-insoluble molecules within ABC triblock terpolymers†

Received 00th January 20xx,
Accepted 00th January 20xx

DOI: 10.1039/x0xx00000x

Rintaro Takahashi,*[a‡] Shotaro Miwa,[a‡] Carsten Rössel,[b] Shota Fujii,[a] Ji Ha Lee,[a] Felix H. Schacher,[b] Kazuo Sakurai*[a]

Polymeric micelles have been extensively studied as nanoscale drug carriers. Knowing how the encapsulation of drugs alters the micellar structure is one of the most important issues for the biomedical application of amphiphilic block copolymers. However, little is known so far about the structural changes of micelles undergo upon loading with water-insoluble guests. Herein, we investigate the micellar morphology of ABC triblock terpolymers after loading with various water-insoluble molecules (naphthalene and derivatives as drug-equivalent model molecules). The triblock terpolymer features a poly(ethylene oxide) (PEO) block, a poly(allyl glycidyl ether) segment which has been functionalized with carboxylic acid moieties ($PAGE_{COOH}$), and poly(*tert*-butyl glycidyl ether) (P*t*BGE) as hydrophobic block. Structural analysis by small-angle X-ray scattering (SAXS) and cryogenic and conventional transmission electron microscopy (TEM) found that a morphological transition from spherical micelles to vesicles (polymersomes) was induced by loading the guest molecules at pH 4, whilst the spherical and prolate morphologies remained unchanged upon loading at pH 6 and 8. This study highlights dynamics and morphological changes of polymeric micelles upon loading with guest molecules.

Introduction

Drug delivery systems using polymeric micelles/vesicles are of great interest, and many researchers have studied the fundamental properties of drug-loaded micelles from various perspectives, in pursuit of their practical use.[1–6] In particular, clarifying the structure of drug-loaded micelles is a critical issue, as it has been reported that the size[7,8] and shape[9–11] of nanoparticles significantly influence their cellular uptake efficiency and biodistribution. Information on the internal structure of drug-loaded micelles is also important.[12–21] For example, Press *et al.*[12] demonstrated that the pharmacokinetics and biodistribution were affected by the location of a drug within the micelle. In addition, Akiba and coworkers[13–16] investigated where water-insoluble guest molecules, which can be considered as a model drug, are located within block copolymer micelles in aqueous solution by using anomalous small-angle X-ray scattering (ASAXS). These studies revealed that highly hydrophobic molecules show a tendency to be loaded into the centre of the micellar core. In contrast, moderately hydrophobic molecules are likely to be localized in the vicinity of the core–corona interface. However, little attention has so far been devoted to the effect of the loading of hydrophobic (water-insoluble) guest molecules on the micellar morphology as it often has been postulated that this is not changed at all during the loading process.

In this study, we directed the focus on the resulting micellar morphology of a poly(ethylene oxide)-*block*-poly(allyl glycidyl $ether_{COOH}$)-*block*-poly(*tert*-butyl glycidyl ether) (PEO-*b*-$PAGE_{COOH}$-*b*-P*t*BGE triblock terpolymer upon loading with naphthalene derivatives (Chart 1a).[22,23] We[23] previously studied the self-assembly of this triblock terpolymer in water

Chart 1 Chemical structures of PEO-*b*-$PAGE_{COOH}$-*b*-P*t*BGE[a] (a), and model guest molecules used in this study: Nap (b), NapAc (c), and NapAm (d)

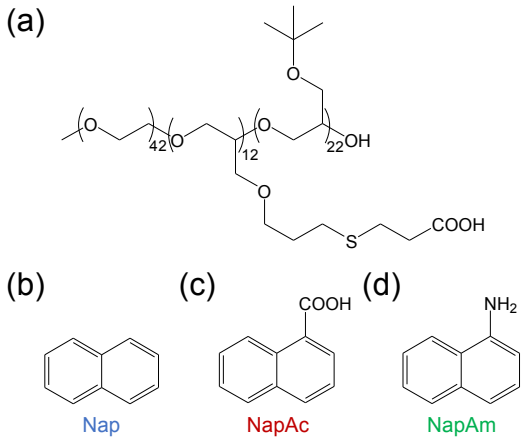

[a] *Department of Chemistry and Biochemistry, University of Kitakyushu, 1-1, Hibikino, Wakamatsu-ku, Kitakyushu, Fukuoka, 808-0135, Japan. (R.T.) E-mail: r-takahashi@kitakyu-u.ac.jp., (K.S.) E-mail: sakurai@kitakyu-u.ac.jp.*
[b] *Institute of Organic Chemistry and Macromolecular Chemistry, Friedrich Schiller University Jena, Lessingstraße 8, D-07743 Jena, Germany, and Jena Center for Soft Matter (JCSM), Friedrich Schiller University Jena, Philosophenweg 7, 07743 Jena, Germany.*
† Electronic Supplementary Information (ESI) available: Scattering function of the polymersome bilayer. See DOI: 10.1039/x0xx00000x
‡ These authors equally contributed to this work.

as selective solvent without any guest molecules, and revealed that spherical micelles are formed at pH 4. By increasing the pH, the morphology is changed to a rather prolate shape. The material features side-chain carboxylic acids in the middle block and therefore net charge and charge density depend on the pH of the surrounding medium. Even more, this directly influences the overall hydrophilicity of the micelles and allows electrostatic interactions with additional ionic substances. Typical anticancer drugs such as doxorubicine feature both hydrophobic and ionic parts and, therefore, we selected non-ionic and ionic water-insoluble guest molecules as models: naphthalene (NAP), 1-naphthylamine (NapAm), and 1-naphthoicacid (NapAc, Chart 1b–d). In this contribution, we investigated the morphology of these micelles with the guest molecules loaded in aqueous solution at different pH by using small-angle X-ray scattering (SAXS), cryogenic transmission electron microscopy (cryo-TEM) and conventional TEM experiments.

Results and discussion

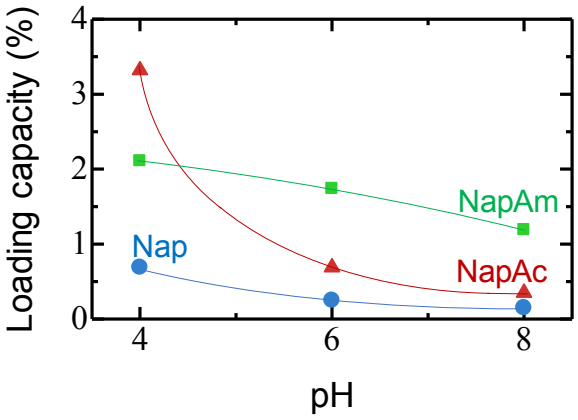

Fig. 1 Loading capacity of the herein used guest molecules as a function of pH in 50 mM Britton–Robinson buffer. Blue, red, and green symbols represent the data for Nap, NapAc, and NapAm, respectively.

We expect that upon self-assembly in the presence of Nap, NapAc or NapAm the guest molecules are encapsulated within the hydrophobic core of the triblock terpolymer micelles. Prior to demonstrating such structural data, we show the loading capacity of each guest molecule, estimated at different pH of 4, 6, and 8 by UV measurements, in Fig. 1. Here, the loading capacity is defined as $W_{guest}/(W_{guest} + W_{polym})$, with W_{guest} representing the weight of the guest molecule and W_{polym} representing the weight of the triblock terpolymer in the micelle. In all three cases, we observed a higher loading capacity within the resulting micelles with decreasing pH. As previously reported,[23] both aggregation number and hydrodynamic radius increased in the order of pH 4 > 6 > 8, also providing an explanation for a higher loading capacity.[6] Nap as the most hydrophobic guest molecule also exhibited the lowest loading capacity. Meanwhile, in the cases of ionically modified naphthalenes (*viz.*, NapAc and NapAm), the loading capacity was found to be distinctly higher. As the miscibility between the guest molecule and the core-forming block is known to influence the loading capacity,[6] the above results suggest that the ionically modified naphthalenes show higher miscibility compared to Nap. Hereby, the loading capacity of NapAc decreases with increasing pH value, presumably due to decreasing solubility of NapAc (partition coefficient) in water, as the pKa of NapAc is known to be 3.69.[24]

We carried out SAXS measurements under conditions where the micelles were fully loaded, as the results are shown in Fig. 2 (Fig. 2, also in the absence of guest molecules at different pH values). In this figure, $I(q)$ denotes the differential scattering cross-section as a function of the magnitude of the scattering vector (q).

Although previously reported in detail,[23] the findings from the SAXS data in the absence of the guest molecules are summarized as follows: The SAXS profile (orange circles) at pH 4 exhibited a plateau at the low-q region and clear oscillations at the higher-q region (q ~ 0.3–1.5 nm^{-1}), which diminish with increasing pH. These features as well as the fitting results[23] indicate that spherical micelles are formed at pH 4 and change into prolate with increasing pH. This morphological change can be explained by the interfacial energy (*c.f.,* Refs. 23 and 25).

It is emphasized that by loading the guest molecules into the micelle the SAXS profiles were remarkably changed at pH 4 (Fig. 2a). The major increase in $I(q)$ in the low-q region hints towards an increase in the molar mass of the scattering objects (much more than the increment due to the added guest molecules). The low-q region exhibits a steeper q-dependence and the relationship of $I(q) \sim q^{-2}$, which indicates that a plate-like structure is formed. Slight oscillations at the lower-q region may be caused by the form factor of the shell-like structure; in other words, polymersomes (not disklike micelles) may be formed. This was confirmed by TEM, as shown later. Meanwhile, in the higher-q regime, a sharp minimum (oscillation) was observed at q ~ 0.4 nm^{-1}, confirming that this structure is well defined; that is, the layer thickness of the polymersome (or disk-like micelle) has a narrow dispersity.

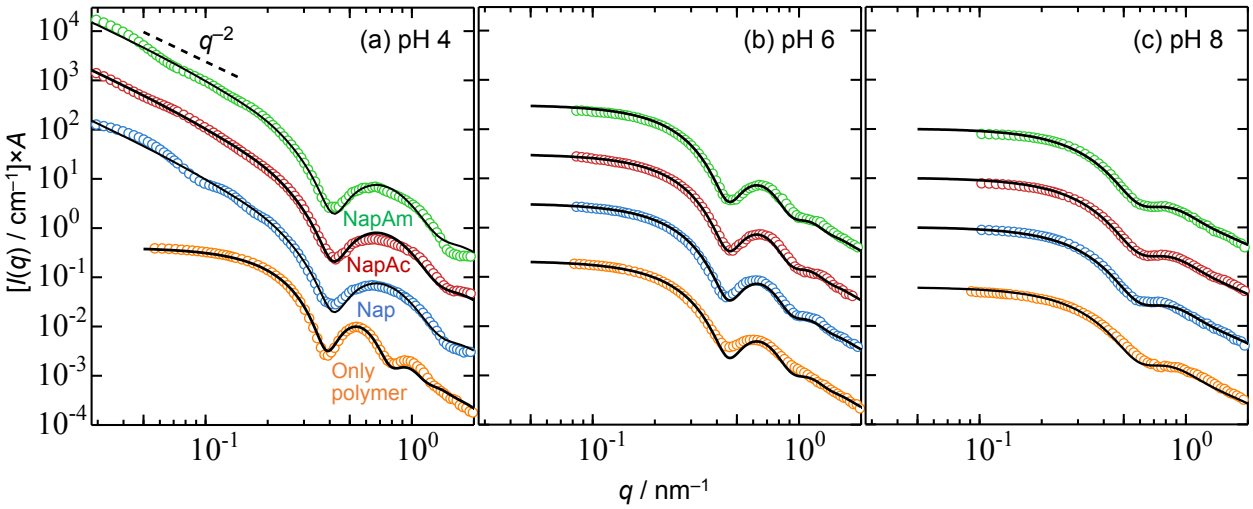

Fig. 2 SAXS profiles of PEO-*b*-PAGE$_{COOH}$-*b*-P*t*BGE without guest molecules (orange symbols), and with Nap (blue symbols), NapAc (red symbols), and NapAm (green symbols) in 50 mM Britton–Robinson buffer at pH 4 (a), pH 6 (b), and pH 8 (c). The polymer concentration was 0.003 g/mL. Each plot was shifted vertically for clarity (Shift factors of A = 1 for only polymer, A = 10 for Nap, A = 10^2 for NapAc, and A = 10^3 for NapAm). Black solid curves represent the fitted model curves. The black solid curves represent the fitted curves by the bilayer model (eq 1; for pH 4 with the guest molecules), the spherical micelle model[23] (for pH4 without guest molecules and pH 6), and the ellipsoidal micelle model[23] (for pH 8).

We therefore calculated the model scattering form factor [$P_{bilayer}(q)$] for a bilayer vesicle with a core of homogeneous density and the Gaussian corona chains attached to the core, as illustrated in Fig. 3, which can be expressed by[26–28]

$$P_{bilayer}(q) = \left[f_{core} E_{core}(q) - (1 - f_{core}) E_{corona}(q) \right]^2 P_0(q) + \frac{(1 - f_{core})^2}{N_{agg}} \left[E^2_{chain}(q) - E^2_{corona}(q) P_0(q) \right] \quad (1)$$

Here, $P_0(q)$ denotes the form factor of an infinitely thin shell with the radius of R_{ves} (eq S1), and forms the framework of the shell-like structure (vesicle) producing the feature of $I(q) \sim q^{-2}$. $E_{core}(q)$, $E_{corona}(q)$, and $E_{chain}(q)$ denote the scattering amplitudes from the core, corona, and individual corona chain (eqs S2–S4), respectively, which consider the cross-sectional structure and produce the oscillations in the high-q regime. In the modeling, we neglected the structure factor and used the relation of $I(q) \propto P_{bilayer}(q)$ because of the dilute concentration. The following parameters are present in the model: core thickness (L), radius of gyration of the corona chain ($\langle S^2 \rangle_{corona}^{1/2}$), aggregation number ($N_{agg}$), R_{ves}, and contrast of the core region defined by f_{core} = $w_{core}\Delta\rho_{core}/(w_{core}\Delta\rho_{core} + w_{corona}\Delta\rho_{corona})$ where w_i and $\Delta\rho_i$ denote the weight fraction and the excess electron density of the core (i = core) and corona (i = corona) parts. The model does not take into account the dispersity in L.

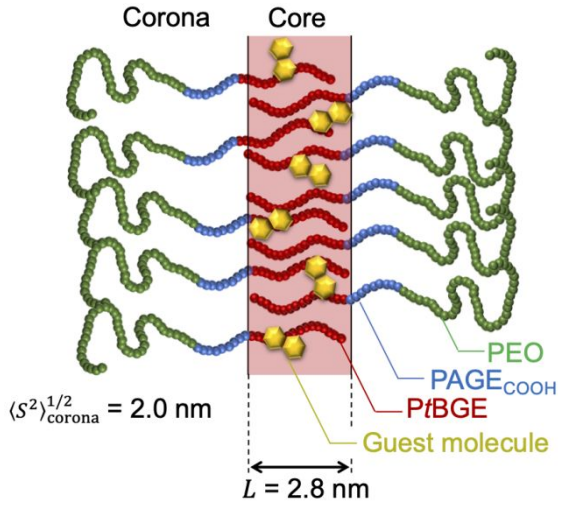

Fig. 3 Schematic illustration of the cross-section of the polymersome bilayer.

As previously shown,[23] the core domain of the micelle (vesicle) consists of the P*t*BGE block, and the PAGE$_{COOH}$ and PEO block chains behave as corona chains (*cf.* Fig. 3), albeit the hydrophilicity of PAGE$_{COOH}$ depends on the pH value. We note that the electron density of the P*t*BGE block is slightly lower than that of the solvent (*i.e.,* $\Delta\rho_{core}$ is negative and its absolute value is rather small). Compared to the P*t*BGE block, PAGE$_{COOH}$ and PEO block chains feature higher electron densities, and both are comparable (*i.e.,* $\Delta\rho_{corona}$ is positive and its absolute value is significantly higher than that of $\Delta\rho_{core}$).

This model fits well to the experimentally obtained data points for the micelle with the guest molecules loaded at pH 4, as represented by the black solid curves in Figure 2. The parameters used in the fitting are listed in Table 1, and did not significantly depend on the type of the guest molecule. The absolute f_{core} values of the polymersomes (with the guest molecules loaded) are smaller than those of the spherical micelles (without any guest molecules, Table 1). This may reflect that the guest molecules, with higher electron density than P*t*BGE block, are loaded into the core domain and increase the electron density. Further, the model scattering function assuming a homogeneous electron density in the core

Table 1 Parameters used for the fitting of the SAXS profiles

pH	Morphology	L or $2R_{core}$ / nm	$\langle S^2\rangle_{corona}^{1/2}$/nm	f_{core}
4 (without guest molecule)	Spherical micelle	5.9	2.0 ± 0.2	– 0.07 ± 0.02
4 (with guest molecule)[a]	Polymersome	2.8	2.0 ± 0.2	– 0.02 ± 0.01
6[b]	Spherical micelle	4.7	2.0 ± 0.2	– 0.07 ± 0.02
8[b]	Prolate micelle	4.4[c], (7.0)[d]	2.0 ± 0.2	– 0.07 ± 0.02

[a]The parameters used for the fitting were independent of the type of the guest molecule. [b]For pH 6 and 8, the SAXS profiles were fitted by the same model regardless of whether or not the guest molecule was loaded. [c]Double of the semi-minor axis. [d]Double of the semi-major axis.

domain adequately fitted to the experimentally obtained data, suggesting that the guest molecules are uniformly distributed within the core domain in all cases. The $\langle S^2\rangle_{corona}^{1/2}$ values were 2.0 ± 0.2 nm irrespective of whether guest molecules were present or not, which further supports the assumption that the guest molecules locate within the core.

The value of L = 2.8 nm was smaller than that of the core diameter of the spherical micelle ($2R_{core}$ = 5.9 nm) at pH 4 without the presence of guest molecules. The following trend was often reported for various polymers:[25,29–34] The core thickness (diameter) is larger in the order of spherical micelle > cylindrical micelle > polymersome. This trend can be interpreted in view of the interfacial energy for each morphology, as described elsewhere,[25] and the core thickness in the present case agrees well with that general trend. The general loading capacity for the guest molecules was not high (< 5%), so the thickening of the core by the guest molecules should be small in comparison with the contribution of the interfacial energy. As just described, information about the cross-section of the bilayer could be derived from the SAXS data. However, since no plateau (Guinier region) was observed in the low q-regime, we could not determine the overall size, namely, the R_{ves} and N_{agg} values; thus, these values were assumed to be 200 nm and 3.5 × 10^5, respectively, in the fitting.

Meanwhile, at pH values of 6 and 8, the SAXS profiles remained unchanged upon loading the guest molecules (Fig. 2b and 2c). At pH 6, the spherical micelle model[26,27] could fit well to all of the SAXS profiles regardless of whether or not the guest molecules were loaded. Although the prolate micelle model[28] fitted to the experimentally obtained data at pH 6 in previous work,[22] the spherical model fitted better in the present case. This might be related to a different type of buffer in the present case. All of the SAXS profiles at pH 8 could be fitted by the prolate micelle model,[28] also irrespective of whether or not the guest molecules were present. The equations for the spherical and prolate micelles as well as the detailed strategy in the fitting were described in a previous paper,[23] and Table 1 lists the parameters used in the fitting. The reason why the morphological change takes place at pH 4 but not at pH 6 and 8 will be discussed later.

The morphology of the micelles at different pH was also investigated by cryo-TEM. Fig. 4a–c displays the obtained images for the NapAc-loaded cases at pH 4–8, respectively. At pH 4, polymersomes can be observed whereas at pH 6 and 8 rather small spherical micelles are visible. Similar structures were observed earlier[23] in the absence of any guest molecules at pH 4 and 8. The presence of polymersomes can also be confirmed by conventional TEM with sodium phosphotungstate staining as shown in Figure 4d and 4e. TEM experiments for Nap could not be performed, but the SAXS profile in case of Nap was almost identical to those of NapAc and NapAm; therefore, we can postulate that polymersomes are also formed by loading Nap at pH 4.

The thickness of the bilayer was estimated to be 10 ± 1 nm from the TEM images in case of both NapAc and NapAm, which is almost equal to the thickness of the model to fit the SAXS profiles ($2\langle S^2\rangle_{corona}^{1/2}$ + L + $2\langle S^2\rangle_{corona}^{1/2}$ = 10.8 nm). However, the overall size (radius) of the polymersomes in Fig. 4a is smaller than in Figure 4d. This can be explained as follows: Vesicles can grow *via* collision and fusion processes,[35] and hence the radius may depend on the time since preparation of the respective sample.[36,37] Thus, we do not further discuss the polymersome radius and note that the polymersomes did not precipitate for at least one month after preparation.

In general, morphological transitions of block copolymer micelles and vesicles can be interpreted in terms of the packing parameter as defined by[38]

$$\lambda_p = \frac{v}{a_0 l_c} \quad (2)$$

with the effective volume of the core-forming block chain (v), the area per chain of the core–corona interface (a_0), and the length of the core-forming block chain (l_c). It is known that, in the case of λ_p < 1/3, the spherical morphology is stable, at 1/3 < λ_p < 1/2 a cylindrical morphology should be observed, and at 1/2 < λ_p disk-like (vesicular) morphologies are preferentially formed. In the present case, the polymer in the absence of any guest molecules forms spherical micelle at pH = 4, indicating that the λ_p is small (< 1/3). By loading the water-insoluble guest molecules into the core domain, v and thus λ_p should increase, resulting in a morphological transition. Although the herein presented SAXS and TEM studies focus on the condition where the highest amount of guest molecules was loaded, if the loading amount were decreased, λ_p could be in the range between 1/3 and 1/2, and thus cylindrical micelles might be formed. On the other hand, at pH 6 and 8, the spherical and prolate morphologies were not changed after loading. At these pH values, the electrostatic repulsion between the $PAGE_{COOH}$ block chains may be dominant due to the increased degree of ionization of the carboxylic groups; it should lead to large a_0.

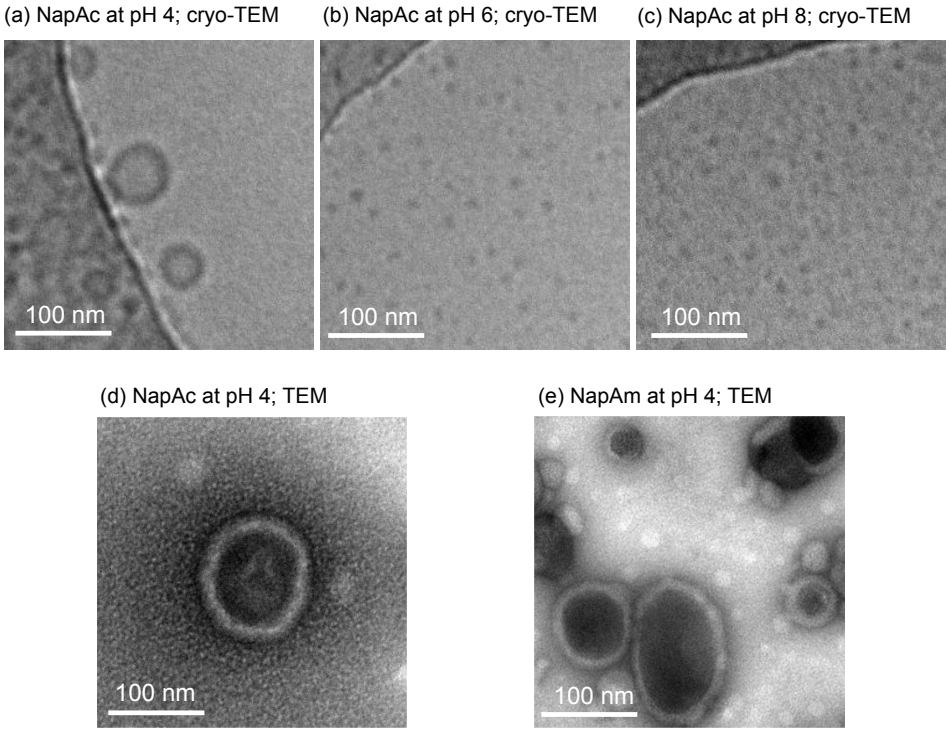

Fig. 4 Representative cryo-TEM images at pH 4 (a), pH 6 (b), and pH 8 (c) with loading of NapAc, and conventional TEM images at pH 4 with loading of NapAc (d) and NapAm (e). The solutions were prepared at a polymer concentration of 0.003 g/mL in 50 mM Britton–Robinson buffer. See also Figure 6 in Ref. 23, where cryo-TEM images for the micelle in the absence of guest molecules are displayed.

Additionally, the loading capacity of the guest molecules is smaller (Fig. 1). Thus, the λ_p values may still be low due to large a_0, and the morphological transition did not occur upon loading the guest molecules at pH 6 and 8. In other words, the interaction between corona chains plays a key role for an eventual morphological transition during loading.

Several studies reported morphological changes upon loading of water-insoluble guest molecules for polymeric micelles, but the reason for this change was not always discussed in detail.[39–45] Within this literature, as far as the authors know, there is only one report on polymersome formation induced by drug loading. Specifically, Cao *et al.*[43] investigated the self-assembly of a block copolymer poly(1-*O*-methacryloyl-*β*-$_D$-fructopyranose)-*block*-poly(methyl methacrylate) upon loading of curcumin. They found that curcumin was loaded into the corona region of the micelle despite its hydrophobicity (this was also reported by another group[19]), and the loading induced the morphological transition from cylindrical micelle to the polymersome, although the actual reason was not discussed. Contrary to their study, in the present case, the water-insoluble guest molecules locate in the core domain, and thus, the core volume was enlarged to induce polymersome formation. The water-insoluble molecules normally show a tendency to locate in the core domain (or the vicinity of the core–corona interface);[13–16] therefore, we believe that the phenomenon of polymersome formation upon loading of water-insoluble guest molecules might be applicable too many other cases where block copolymer nanocarriers are investigated.

Conclusions

We demonstrated that the morphological transition from spherical micelle to polymersome was induced by loading water-insoluble guest molecules at pH 4. The SAXS data can be adequately described by the model assuming that the guest molecules are uniformly distributed within the bilayer core domain. This transition may occur because the guest molecules enlarge the micellar core volume and thus change the packing parameter. On the other hand, at pH 6 and 8, the spherical and prolate morphologies of the triblock terpolymer micelles were maintained even if the guest molecules were loaded, because the electrostatic repulsion between the middle blocks ($PAGE_{COOH}$), rather than the effect of the loading, was dominant in determining the micellar morphology. This study offers an unprecedented strategy to prepare polymersomes through adjusting the packing parameter by water-insoluble guest molecules and further adds to a general understanding of cargo-carrier interactions and resulting effects on morphology and stability of block copolymer nanostructures.

Experimental

Materials. The triblock copolymer (PEO-*b*-PAGE$_{COOH}$-*b*-P*t*BGE) used in this study has been reported previously.[22,23] Table 2 lists the molecular characteristics of the triblock terpolymer. Nap, NapAc, and NapAm were purchased from Tokyo Chemical Industry (Tokyo, Japan) and used as received. Water was deionized using a Millipore Milli-Q system.

Preparation of micelles with the water-insoluble guest molecules loaded. The triblock terpolymer sample and each guest molecule with a weight ratio of 10:1 were dissolved in tetrahydrofuran (THF) in a graduated cylinder. Water was poured into the solution, followed by the removal of THF by gentle heating to *ca.* 50 °C and reduced pressure with stirring for at least 10 h. Water was further poured into the solution to adjust the volume. The solution was mixed with each aqueous buffer solution to adjust the pH. The buffer solutions were composed of boronic acid, phosphoric acid, acetic acid, and NaOH (Britton–Robinson buffer).[46,47] The excess drug was removed by ultrafiltration. In the following measurements, the mass concentration of the triblock terpolymer was 0.003 g/cm^3 and the molar concentration of the buffer was 50 mM. The pH values of 4, 6, or 8 was checked using a pH meter.

Estimations of the loading capacity. The UV measurements were conducted for the polymer in aqueous buffer solution to estimate the absorption coefficient by a V-630 spectrophotometer (JASCO, Tokyo, Japan) at 25 °C. We also estimated the absorption coefficient for each guest molecule in aqueous buffer solution containing sodium dodecyl sulfate as the solvent and the polymer in aqueous buffer solution. After that, the UV absorbance for the micelle with the guest molecules loaded was measured, followed by subtracting the contribution of the polymer. From this result, the concentration of the drug in the solution was obtained with each absorption coefficient. Note that naphthalene and its derivatives used in this study have maxima in their UV spectrum, and the position of the peak in the UV spectra remained unchanged if they were loaded into the triblock terpolymer micelles.

SAXS. SAXS measurements were carried out at the BL40B2 and BL03XU beamlines, SPring-8, Sayo, Japan. The sample-to-detector distance was selected to be 4 and 1 m in this study. The sample solution in a quartz capillary cell with a diameter of 2 mm was exposed to the X-ray with a wavelength (λ) of 0.1 nm. The sample temperature was maintained at 25 °C during the X-ray exposure. The scattering intensity was recorded using a PILATUS detector (Dectris, Baden, Switzerland). By taking the azimuthal average for the obtained 2D image data and subtracting the background scattering, the excess scattering intensity was obtained as a function of q. q is defined by $q \equiv (4\pi/\lambda)\sin(\vartheta/2)$ where ϑ is the scattering angle. The excess scattering intensity was normalized to $I(q)$ by a standard method (scattering intensity from water was used).[48] In the obtained SAXS profiles, the data points influenced by the beam stopper were removed. Further, the measurement of $I(q)$ in the low-q region is difficult in cases of low contrast and small-size particles in solution because the background scattering is higher at the lower-q region, which leads to a lower S/N ratio. Thus, highly rough data points at the lower-q region were removed from the SAXS profiles.

Table 2 Molecular characteristics of the synthesized triblock terpolymer[23]

$M_{n,1}{}^a$	$M_{w,1}{}^b$	$M_{w,1}/M_{n,1}{}^c$	$N_{PEG,n}{}^d$	$N_{PAGECOOH,n}{}^d$	$N_{PtBGE,n}{}^d$
7400	8000	1.08	42	12	22

[a]Number-average molecular weight, determined by ^{1}H NMR. [b]Weight-average molecular weight, calculated from $M_{n,1}$ and $M_{w,1}/M_{n,1}$. [c]Dispersity index, determined by size exclusion chromatography in chloroform with PEO calibration. [d]Number-average degree of polymerization of each block chain, determined by ^{1}H NMR.

Cryo- and conventional TEM. Cryo-TEM measurements were conducted using a FEI Tecnai G^2 20 cryo-transmission electron microscope with an acceleration voltage of 200 kV.[23] Each sample solution for the cryo-TEM experiment was plunge-frozen by immersion it into liquid ethane. The samples were prepared on Quantifoil grids (3.5/1) after cleaning by argon plasma treatment for 120 s. The solutions at a volume of 8.5 μL of were blotted using a Vitrobot Mark IV.

Conventional TEM observations were also performed using a JEM-3010 instrument (JEOL Ltd., Tokyo, Japan) with an accelerating voltage of 100 kV. In the sample preparation for the conventional TEM measurement, each solution was dropped on a copper grid and wiped away. After that, an aqueous solution of sodium phosphotungstate (0.2wt %) was also dropped to stain the sample, followed by being wiped away.

Conflicts of interest

There are no conflicts to declare.

Acknowledgements

The SAXS experiments were carried out at SPring-8 under the approval of JASRI with proposal numbers 2017B1481, 2017A1414, 2017A1238, and 2019A7231. This research was supported by a Grant-in-Aid from CREST-JST (JPMJCR1521), the Deutsche Forschungsgemeinschaft for funding (SCHA1640/12-1) and also within the framework of the collaborative research centre PolyTarget (SFB1278, project C03). The TEM facilities of the Jena Center for Soft Matter (JCSM) were established with a grant from the German Research Council (DFG) and the European Fonds for Regional Development (EFRE). We thank Moritz Köhler for performing the cryo-TEM measurements.

References

1 H. Cabral, K. Miyata, K. Osada and K. Kataoka, *Chem. Rev.,* 2018, **118,** 6844.
2 M. Karimi, A. Ghasemi, P. S. Zangabad, R. Rahighi, S. M. M. Basri, H. Mirshekari, M. Amiri, Z. S. Pishabad, A. Aslani, M. Bozorgomid, D. Ghosh, A. Beyzavi, A. Vaseghi, A. R. Aref, L. Haghani, S. Bahrami and M. R. Hamblin, *Chem. Soc. Rev.,* 2016, **45,** 1457.
3 H. Maeda, K. Tsukigawa and J. Fang, *Microcirculation,* 2016, **23,** 173.
4 J. C. Brendel and F. H. Schacher, *Chem. - Asian J.* 2018, **13,** 230.
5 X. Hu, Y. Zhang, Z. Xie, X. Jung, A. Bellotti, Z. Gu, *Biomacromolecules,* 2017, **18,** 649.

6 J. Liu, H. Lee and C. Allen, *Curr. Pharm. Des.,* 2006, **12,** 4685.
7 H. Cabral, Y. Matsumoto, K. Mizuno, Q. Chen, M. Murakami, M. Kimura, Y. Terada, M. R. Kano, K. Miyazono, M. Uesaka, N. Nishiyama and K. Kataoka, *Nat. Nanotechnol.,* 2011, **6,** 815.
8 R. P. Brinkhuis, K. Stojanov, P. Laverman, J. Eilander, I. S. Zuhorn, F. P. J. T. Rutjes and J. C. M. van Hest, *Bioconjug. Chem.,* 2012, **23,** 958.
9 S. Dasgupta, T. Auth and G. Gompper, *Nano Lett.,* 2014, **14,** 687.
10 T. Pelras, H. T. T. Duong, B. J. Kim, B. S. Hawkett and M. Müllner *Polymer,* 2017, **112,** 244.
11 M. Müllner, K. Yang, A. Kaur and E. J. New, *Polym. Chem.,* 2018, **9,** 3461.
12 A. T. Press, A. Ramoji, A. C. Rinkenauer, M. vd Lühe, J. Hoff, M. Butans, C. Rössel, C. Pietsch, U. Neugebauer, F. H. Schacher, and M. Bauer, *NPG Asia Mater*., 2017**, 8,** e444.
13 Y. Sanada, I. Akiba, K. Sakurai, K. Shiraishi, M. Yokoyama, E. Mylonas, N. Ohta, N. Yagi, Y. Shinohara and Y. Amemiya, *J. Am. Chem. Soc.,* 2013, **135,** 2574.
14 R. Nakanishi, M. Kinoshita, S. Sasaki and I. Akiba, *Eur. Polym. J.,* 2016, **81,** 634.
15 R. Nakanishi, G. Machida, M. Kinoshita, K. Sakurai and I. Akiba, *Polym. J.,* 2016, **48,** 801.
16 S. Sasaki, G. Machida, R. Nakanishi, M. Kinoshita and I. Akiba, *Polymers,* 2018, **10,** 180.
17 I. Akiba, N. Terada, S. Hashida, K. Sakurai, T. Sato, K. Shiraishi, M. Yokoyama, H. Masunaga, H. Ogawa, K. Ito and N. Yagi, *Langmuir,* 2010, **26,** 7544.
18 M. Callari, P. L. De Souza, A. Rawal, M. H. Stenzel, *Angew. Chem. Int. Ed.,* 2017, **56,** 8441.
19 A.-C. Pöppler, M. M. Lübtow, J. Schlauersbach, J. Wiest, L. Meinel and R. Luxenhofer, *Angew. Chem. Int. Ed.,* 2019, **58,** 18540.
20 Sochor, B.; Düdükcü, Ö.; Lübtow, M. M.; Schummer, B.; Jaksch, S.; Luxenhofer, R. *ChemRxiv Preprint* https://doi.org/10.26434/chemrxiv.10259552.v1.
21 Z. Li, T. I. Lenk, L. J. Yao, F. S. Bates and T. P. Lodge, *Macromolecules,* 2018, **51,** 540–551.
22 M. J. Barthel, A. C. Rinkenauer, M. Wagner, U. Mansfeld, S. Hoeppener, J. A. Czaplewska, M. Gottschaldt, A. Traẅger, F. H. Schacher and U. S. Schubert, *Biomacromolecules,* 2014, **15,** 2426.
23 S. Miwa, R. Takahashi, C. Rössel, S. Fujii, J. H. Lee, F. H. Schacher, and K. Sakurai, *Langmuir,* 2018, **34,** 7813.
24 H. C. Brown, D. H. McDaniel and O. Hafliger, in E. A. Braude and F. C. Nachod ed., *Determination of Organic Structures by Physical Methods*, Academic Press, New York, 1955.
25 R. Takahashi, T. Sato, K. Terao, and Yusa, S., *Macromolecules,* 2015, **48,** 7222.
26 J. S. Pedersen, M. Gerstenberg, *Macromolecules,* 1996, **29,** 1363.
27 J. S. Pedersen, *J. Chem. Phys.,* 2001, **114,** 2839.
28 J. S. Pedersen, *J. Appl. Cryst.,* 2000, **33,** 637.
29 R. Takahashi, T. Narayanan, S. Yusa, and T. Sato, *Macromolecules,* 2018, **51,** 3654.
30 Y.-Y. Won, A. K. Brannan, H. T. Davis and F. S. Bates, *J. Phys. Chem. B,* 2002, **106,** 3354.
31 S. Jain and F. S. Bates, *Macromolecules* **2004,** *37,* 1511–1523.
32 P. Bhargava, J. X. Zheng, P. Li, R. P. Quirk, F. W. Harris and S. Z. D. Cheng, *Macromolecules,* 2006, **39,** 4880.
33 J. Bang, S. Jain, Z. Li, T. P. Lodge, J. S. Pedersen, E. Kesselman and Y. Talmon, *Macromolecules,* 2006, **39,** 1199.
34 L. Zhang, A. Eisenberg, *Macromolecules,* 1999, **32,** 2239.
35 T. M. Weiss, T. Narayanan, C. Wolf, M. Gradzielski, P. Panine, S. Finet and W. I. Helsby, *Phys. Rev. Lett.,* 2005, **94,** 038303.
36 V. Guida, *Adv. Colloid. Interface Sci.,* 2010, **161,** 77.
37 R. Bleul, R. Thiermann and M. Maskos, *Macromolecules,* 2015, **48,** 7396.
38 J. N. Israelachvili, *Intermolecular and Surface Forces, 3rd ed.;* Academic Press: 2011.
39 M. Valero and C. A. Dreiss, *Langmuir,* 2010, **26,** 10561.
40 M. Khimani, R. Ganguly, V. K. Aswal, S. Nath and P. Bahadur, *J. Phys. Chem. B,* 2012, **116,** 14943.
41 A. Schulz, S. Jaksch, R. Schubel, E. Wegner, Z. Di, Y. Han, A. Meister, J. Kressler, A. V. Kavanov. R. Luxenhofer, C. M. Papadakis and R. Jordan, *ACS Nano,* 2014, **8,** 2686.
42 C. Gao, J. Zhao, F. Chen, M. Lu, Y. Y. Khine, A. Macmillan, C. J. Garvey and M. H. Stenzel, *Chem. Mater.,* 2018, **30,** 5227.
43 F. L. Dévédec, S. Her, K. Vogtt, A. Won, X. Li, G. Beaucage, C. Yip and C. Allen, *Nanoscale,* 2017, **9,** 2417.
44 H. Luo, K. Jiang, X. Liang, C. Hua, Y. Li and H. Liu, *Colloid. Surf. A,* 2019, **572,** 221.
45 A. S. Mikhail and C. Allen, *Biomacromolecules,* 2010, **11,** 1273.
46 H. T. S. Britton and R. A. Robinson, *J. Chem. Soc.,* 1931, 1456.
47 C. Mongay and V.. Cerda, *Anali di Chemica,* 1974, **64,** 409.
48 D. Orthaber, A. Bergmann and O. Glatter, *J. Appl. Crystallogr.,* 2000, **33,** 218.

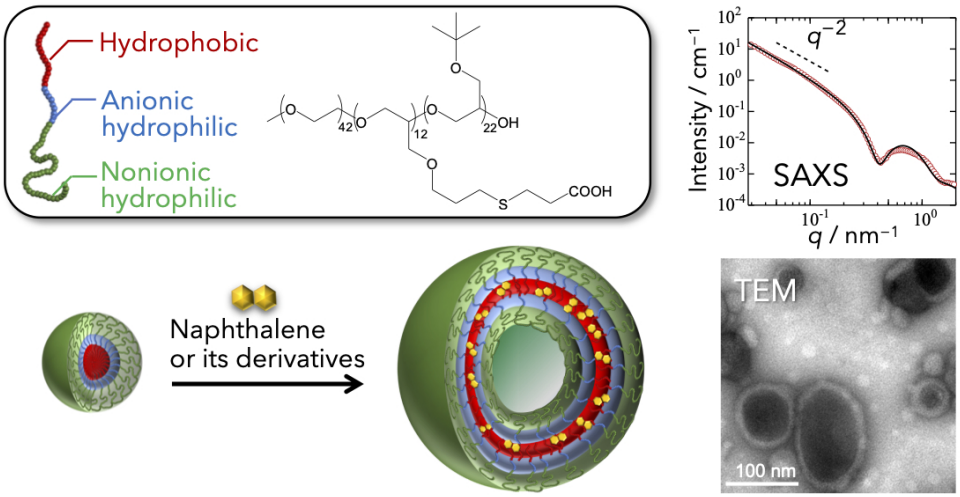

160x80mm (180 x 180 DPI)